Catalysis Today 432 (2024) 114617

Contents lists available at ScienceDirect

Catalysis Today

journal homepage: www.elsevier.com/locate/cattod

O_2 and CO_2 assisted oxidative dehydrogenation of propane using ZrO_2 supported vanadium and chromium oxide catalysts

Rajvikram Singh [a], Sudhir Charan Nayak [b], Raghvendra Singh [a], Goutam Deo [a,c,*]

[a] Department of Chemical Engineering, Indian Institute of Technology Kanpur, Kanpur 208016, India
[b] Department of Chemical Engineering, Indian Institute of Technology (Indian School of Mines), Dhanbad, Dhanbad 826004, India
[c] Department of Sustainable Energy Engineering, Indian Institute of Technology Kanpur, Kanpur 208016, India

ARTICLE INFO

Keywords:
ODH of propane
O_2-ODH
CO_2-ODH
Vanadia
Chromia
Zirconia support

ABSTRACT

Zirconia supported vanadium oxide (vanadia) and chromium oxide (chromia) catalysts of 1–3 wt% of V or Cr were prepared, characterized, and tested for the oxidative dehydrogenation (ODH) of propane (C_3H_8) with O_2 and CO_2. Characterization results reveal that 2.5% metal loading is in slight excess of monolayer loadings for this ZrO_2, which has a surface area of 48 $m^2.g^{-1}$. The reaction results reveal that supported vanadia catalysts are better for O_2-ODH and supported chromia catalyst are better for CO_2-ODH at a reaction temperature of 550 °C. Furthermore, the C_3H_8 conversion and propene (C_3H_6) yield increases with loading and the highest conversion and yield are also achieved at 2.5% metal loading. With higher loadings the conversion and yield decreases, clearly indicating that the surface metal oxide species are more active than their crystalline counterparts. As the contact time increases, for inlet stoichiometric ratios of the reactants for the two reactions, $C_3H_8/CO_2 = 1$ and $C_3H_8/O_2 = 2$, C_3H_8 conversion and C_3H_6 yield both monotonically increase and appear to approach a constant value; however, the difference between C_3H_8 conversion and C_3H_6 yield also increases. The C_3H_6 selectivity during O_2-ODH (~30%) is much lower than C_3H_6 selectivity during CO_2-ODH (86–94%). Furthermore, during CO_2-ODH of propane the conversions of C_3H_8 and CO_2 are similar, and it appears that under the operating conditions used, the dry reforming of propane does not occur. Overall, the CO_2-ODH of propane reaction at 550 °C using stoichiometric ratios of C_3H_8/CO_2 over ZrO_2 supported chromia catalyst provides a better C_3H_6 yield and selectivity, with an additional advantage of converting CO_2.

1. Introduction

Propene continues to be an important intermediate and an essential chemical in the manufacturing sectors, with several uses [1] The demand for propene is increasing rapidly but its supply, through conventional processes, appears to have stagnated over the years [2,3]. In literature, some alternative processes have been proposed and are being implemented and others are being examined for their feasibility [1].

The dehydrogenation of propane (DH) is one of the alternative processes that has been implemented [4]. Though the DH reaction appears most appealing, it is hampered by high energy requirements due to the reaction endothermicity. Further, coke formation that occurs during DH leads to rapid catalyst deactivation. Oxidative dehydrogenation of propane (ODH), using O_2, has been proposed to overcome some of the hurdles faced by the direct dehydrogenation reaction [5]. However, the ODH process has its own drawbacks.

In addition to using O_2 as the oxidant for the ODH of propane reaction, referred to here as O_2-ODH, CO_2, N_2O, and other oxidants have also been used [6]. Considering the interest in the utilizing CO_2, the CO_2-ODH reaction has been receiving much attention [1,7–9]. The stoichiometry and standard heat of reaction for O_2-ODH and CO_2-ODH are given below:

$$C_3H_8 + 0.5O_2 \rightarrow C_3H_6 + H_2O \ \Delta H^o_{rxn} = -188\ kJ/mol\ O_2 - \text{ODH} \quad (1)$$

$$C_3H_8 + CO_2 \rightarrow C_3H_6 + H_2O + CO \ \Delta H^o_{rxn} = +164\ kJ/mol\ CO_2 - \text{ODH} \quad (2)$$

During normal operating conditions, these reactions are accompanied by several side reactions, such as the formation of CO and CO_2 by further oxidation during O_2-ODH, reverse water gas shift reaction, and dry reforming during CO_2-ODH [8].

Supported vanadia and chromia catalysts are often used as catalysts for the DH, O_2-ODH, and CO_2-ODH reactions [10]. For O_2-ODH of

* Corresponding author at: Department of Chemical Engineering, Indian Institute of Technology Kanpur, Kanpur 208016, India.
E-mail address: goutam@iitk.ac.in (G. Deo).

https://doi.org/10.1016/j.cattod.2024.114617
Received 13 January 2024; Received in revised form 18 February 2024; Accepted 27 February 2024
Available online 28 February 2024

propane, supported vanadia catalysts have been extensively studied [11], and supported chromia catalysts are one of the commercial catalysts for the DH of propane [12]. Thus, it would be interesting to compare the supported vanadia and chromia catalysts in the same study for the ODH of propane reaction using O_2 and CO_2 as the oxidants.

Supported vanadia and chromia catalysts are a part of the more general class of catalysts referred to as supported metal oxides. Supported metal oxide catalysts are formed when one metal oxide species is present as an overlayer on a high surface area oxide support [13]. By characterizing these catalysts using several techniques, it has been established that molecularly dispersed surface metal oxide species are present when the loading is below monolayer amounts. Above monolayer amounts bulk or crystalline phases exist along with molecularly dispersed species. With further increase in metal oxide loading, it would be reasonable to speculate that the fraction of molecularly dispersed species decreases and bulk phase increases. Thus, for supported vanadia and chromia species, molecularly dispersed V_xO_y and Cr_mO_n are present below monolayer coverages [14], and above monolayer coverages, V_2O_5 and Cr_2O_3 are the bulk phases present along with the molecularly dispersed species.

Often the molecularly dispersed metal oxide species are found to be the more active phase [15]. To identify the presence of molecularly dispersed species characterization of the catalyst is required. Raman spectroscopy is one of the primary characterization techniques used to identify monolayer coverages, the presence of molecularly dispersed metal oxide species, and other important structural transformations in different environments [16]. Other characterization techniques also provide insights into the nature of the molecularly dispersed metal oxide species in different environments [17].

The oxide support on which the molecularly dispersed phase exists also plays a very important role in the propane conversion and propene yield of supported metal oxide catalyst. Amongst the various oxide supports used to form the supported metal oxide, ZrO_2 supported catalysts are very active for the O_2-ODH [11] and CO_2-ODH [18] of propane reaction. However, studies that compare ZrO_2 supported vanadia and chromia catalysts for the O_2-ODH and CO_2-ODH reactions under similar conditions are, to the best of our knowledge, missing. Using Al_2O_3 as a support, the O_2-ODH reaction at 380 °C with $C_3H_8/O_2/He$ = 9/3/38 revealed that the turnover over frequency of propene formation (TOF_{C3H6}) of vanadia was greater than that for chromia for sub-monolayer catalysts [19]. In contrast, for the CO_2-ODH reaction at 550 °C with $C_3H_8/O_2/N_2$ = 1/3/4, the TOF_{C3H6} for chromia is more than that for vanadia [20]. These studies were carried out under different operating conditions and a proper comparison between the supported vanadia and chromia catalyst for the two ODH of C_3H_8 reactions is difficult to establish. Further, these studies were carried out on Al_2O_3 supported catalysts and not the more active ZrO_2 supported catalysts.

The present work compares the performance of the ZrO_2 supported vanadia and chromia catalysts for the O_2-ODH and CO_2-ODH of propane reactions. The two supported metal oxide catalysts, of loadings that range from below monolayer coverage to an excess of monolayer coverage, are synthesized. Monolayer coverages are identified by Raman spectroscopy and the catalysts are further characterized by: (i) N_2-adsorption for surface area determination, (ii) temperature programmed reduction (TPR) using H_2 (H_2-TPR) to determine the reducibility and H/M ratio (M = V or Cr) and (iii) X-ray photoelectron spectroscopy to determine the oxidation states of vanadium and chromium. A sub-monolayer catalyst of the supported vanadia and supported chromia are tested for O_2-ODH and CO_2-ODH with stoichiometric ratios of C_3H_8 and the oxidant at 550 °C. The more active supported metal oxide catalyst for each ODH reaction is chosen for further studies. Based on the more active supported metal oxide catalyst for each reaction, the effect of metal oxide loading on the reactivity of the corresponding ODH reaction is examined. After identifying the optimum loading, the effect of contact time is analyzed using the same inlet partial pressures of C_3H_8 and O_2 or CO_2, and the highest conversion and yield for each reaction is determined. Finally, the difference between the two reaction-catalyst systems will be discussed and the system that provides the best propene yield is identified.

2. Experimental

2.1. Catalyst synthesis

The supported vanadia and chromia catalysts were prepared using the incipient wetness impregnation (IWI) method using ZrO_2 (Saint Gobain) as the support. The precursor used for vanadia was ammonium meta vanadate (NH_4VO_3) (Loba Chemie) + oxalic acid and, for chromium, the precursor was chromium nitrate nonahydrate ($Cr(NO_3)_3.9\ H_2O$)) (Fluka). Initially, ZrO_2 was pretreated with an incipient volume of solvent, H_2O or H_2O+Oxalic acid, depending on the specific precursor used in the process, and then dried overnight in an oven at around 110°C. The dried ZrO_2 support was calcined, in a step-wise manner at 250 °C for 2 h, 350 °C for 2 h, and finally at 450 °C for 4 h. This pretreated ZrO_2 was used to synthesize the supported catalysts. A precursor solution (precalculated precursor amount + incipient volume of H_2O or H_2O+Oxalic acid) was made corresponding to the metal oxide loading and mixed with the pretreated ZrO_2, forming a paste. This paste was kept in an oven for 12 h at 110 °C and then crushed into powder form. The powder was calcined using the heat treatment protocol for the support. The prepared catalyst was kept in an airtight bottle. The catalysts were referred to as xMZr, where x = metal loading, M = V or Cr, and Zr = ZrO_2.

2.2. Catalyst characterization

2.2.1. Surface area

The specific surface area of the prepared catalyst samples was measured using Autosorb iQ TPX equipment (Quantachrome, USA). It used the multi-point BET method to analyze N_2 adsorption data at –196°C.

2.2.2. Raman spectroscopy

The Raman spectra of the samples were collected using an Acton Spectra Pro 2500i (Princeton Instrument, USA) instrument. The instrument operated with a 532 nm diode-pumped solid-state laser (DPSSL), which delivered 40 mW power at 50% strength. The objective lenses used were 20X and 50X. The spectra were captured under ambient conditions using 20 scans of 2 s each. Since the sample was stationary, there is a possibility of laser-induced heating to occur [21].

2.2.3. X-ray photoelectron spectroscopy (XPS)

The XPS spectra of some fresh and spent catalyst samples were obtained. According to their binding energies, the oxidation states were identified. A NEXSA (Thermoscientific, USA) instrument equipped with an AlKα source for the monochromatic laser was used as the X-ray source. The spectra were obtained at ultra-high vacuum with base pressure $3*10^{-9}$ mbar and at room temperature. The obtained spectra were referenced according to the adventitious carbon peak position at 284.8 eV to avoid charging error. Though the samples were exposed to ambient conditions for a very short time, we have assumed that XPS characterization of the spent catalyst is representative of the catalyst under reaction conditions based on the observations of previous studies [22,23]. To identify the oxidation state, the peaks were deconvoluted by Origin 15 software, following the standard procedures.

2.2.4. Temperature programmed reduction using H_2 (H_2 TPR)

The H_2-TPR profile was obtained for all the prepared catalysts and the ZrO_2 support by loading 60 mg of sample in a U–tube quartz reactor of an AMI 200 (Altamira, USA) set-up. Before reduction, the sample was degassed in an inert argon (Ar) environment at 350 °C for 0.5 h. A temperature of 350 °C was achieved by a ramp rate of 10 °C/min. After

degassing, the sample was cooled to 40°C in the same Ar environment. Thereafter, the reduction was started by using a 10% H_2-Ar mixture flowing at 1.8 L.h^{-1} flow. After stabilizing the flow, the temperature of the catalyst bed was raised to 900°C at a ramp rate of 10 °C/min and maintained at 900 °C for 1 h. The reactor effluent was analyzed using a thermal conductivity detector (TCD), which provided the change in H_2 concentration with temperature. Quantitative determination of the amount of H_2 consumed, H_2-uptake in mol H_2.gm^{-1}, was achieved by using pulse calibration of known amounts of the 10% H_2-Ar mixture.

2.3. Reactivity studies

The prepared catalysts were investigated for the two ODH of propane reactions using a downflow quartz-tube packed-bed reactor. This quartz reactor was placed in a vertical tubular furnace. To assess the temperature of the catalyst bed, a thermocouple was positioned slightly above it. This thermocouple was connected to a PID controller to maintain the catalyst bed at the desired temperatures. Just before the reaction, the catalysts were calcined in situ at 550 °C with oxygen flowing at a rate of 2.4 L.h^{-1}, for 1 h. Subsequently, the reaction line was purged with N_2 for 0.5 h with a constant flow rate of 2.4 L.h^{-1} to remove traces of oxygen. The ODH reactions were performed at the same temperature and atmospheric pressure. The reactant mixture of C_3H_8 and O_2/CO_2 was fed in stoichiometric ratios as given by reactions (1) and (2). The partial pressure of propane was kept at 0.075 atm and N_2 was used as an inert. The total flow rate was maintained at 1.8 L.h^{-1}, except for contact time studies. The exit gas stream was normalized with an independent external stream of CH_4 flowing at a rate of 0.12 L.h^{-1}. The reactor exit gas stream was passed through a condenser to remove any traces of moisture and its composition was analyzed by a gas chromatograph (GC, NUCON 5765). The GC was equipped with a TCD and an FID. The FID was connected to a HySepQ column and the TCD to a Carbosphere column. The peak areas of all the components were detected and used to calculate conversions, yields, and selectivity after using the corresponding calibration factors. The conversions ($X_{C_3H_8}$ and X_{CO_2}), yields ($Y_{C_3H_6}$ and Y_{CO}), propene selectivity ($S_{C_3H_6}$), and turnover frequency of propane ($TOF_{C_3H_8}$) and propene ($TOF_{C_3H_6}$) are defined below.

$$X_{C_3H_8}(\%) = \left(1 - \frac{F_{C_3H_8,out}}{F_{C_3H_8,in}}\right) * 100 \quad (3)$$

$$X_{CO_2}(\%) = \left(1 - \frac{F_{CO_2,out}}{F_{CO_2,in}}\right) * 100 \quad (4)$$

$$Y_{C_3H_6}(\%) = \left(\frac{F_{C_3H_6,out}}{F_{C_3H_8,in}}\right) * 100 \quad (5)$$

$$Y_{CO}(\%) = \left(\frac{F_{CO,out}}{F_{CO_2,in}}\right) * 100 \quad (6)$$

$$S_{C_3H_6}(\%) = \left(\frac{F_{C_3H_6,out}}{F_{C_3H_8,in} - F_{C_3H_8,out}}\right) * 100 \quad (7)$$

$$TOF_{C_3H_6} = \left(\frac{F_{C_3H_6,out}}{W * H_2 - uptake}\right) \quad (8)$$

$$TOF_{C_3H_8} = \left(\frac{F_{C_3H_8,in} - F_{C_3H_8,out}}{W * H_2 - uptake}\right) \quad (9)$$

Where, F_i is the molar flow rate of species i and W is the weight of the catalyst. Here, $W * H_2 - uptake$ is the mols of reducible surface metal oxide present on the supported metal oxide catalyst.

The carbon balance, $\frac{\text{mol C}_{out}}{\text{molC}_{in}} * 100$, was better than 98% for all samples during CO_2-ODH and better than 99% for O_2-ODH. The amount less than 100% was attributed to carbon deposition on the catalyst surface.

3. Result and discussion

Fresh and spent catalysts were characterized and their results are given below.

3.1. Surface area

The specific surface area of all the fresh samples was determined and tabulated in Table 1 along with the surface area of the ZrO_2 support, which was 48 m^2.g^{-1}. As the metal loading is increased, the surface area appears to decrease slightly. Similar trends have been observed previously for ZrO_2 supported chromia [24], and vanadia [25] catalysts.

3.2. Raman Spectroscopy

All the prepared catalysts were characterized with Raman spectroscopy. The Raman spectra of calcined xVZr are shown in Fig. 1. A broad band in the range of 870–1000 cm^{-1} shows the presence of molecularly dispersed surface V_xO_y species. The broadband has been assigned to polyvanadate species that are present on the surface under ambient conditions [26]. Furthermore, the absence of sharper peaks at ~990 and ~780 cm^{-1} suggests that ZrV_2O_7, a bulk compound of ZrO_2 and V_2O_5, is not formed [27,28]. As the loading increased to 2.5%, distinct Raman bands at 994 cm^{-1}, 699 cm^{-1} and 525 cm^{-1} were detected, which are associated with the vibrations of crystalline V_2O_5 in supported catalysts [28–30]. The appearance of the Raman bands for crystalline V_2O_5 suggests that the monolayer loading has been exceeded. Thus, the monolayer coverage lies between 5.1 and 6.7 V-atoms/nm^2, which is close to the monolayer coverages of ~6.8 V-atoms/nm^2 suggested previously [13].

The Raman spectra of calcined xCrZr catalysts are shown in Fig. 2. The major peaks in the Raman spectra due to the molecularly dispersed Cr_mO_n species are observed at 870 cm^{-1} and 1035 cm^{-1}. It appears that these molecularly dispersed species are partially dehydrated under the laser beam, as observed previously [31]. These bands correspond to the surface chromia phase as a molecularly dispersed species [24,32,33]. As the chromium loading increases above 2%, a new Raman band appears at 551 cm^{-1} due to the presence of crystalline Cr_2O_3 [24,32,33], suggesting that the monolayer coverage has been exceeded for the 2.5% loading sample. Similar to the vanadia system, the monolayer coverage of chromia on this ZrO_2 support lies between 5.2 and 6.6 Cr-atom/nm^2, which compares well with the monolayer coverage values of about 5.4 Cr-atom/nm^2 suggested previously for ZrO_2, Al_2O_3, and TiO_2 supported chromia catalysts [24,32].

3.3. XPS data

The XPS scans of freshly calcined catalyst samples of 2.5VZr and 2.5CrZr have been shown in Fig. 1S of supplementary information file. Both the catalysts were scanned in the range of $2p_{3/2}$ and $2p_{1/2}$. The XPS scan of the vanadium catalyst shows that only V^{+5} species is present in the sample since only peaks at 516.85 eV and 524.28 eV for $2p_{3/2}$ and $2p_{1/2}$ are identified [34]. In the case of chromium catalysts, it shows both Cr^{+3} (peak at 515.18 and 523.08 eV) and Cr^{+6} (peaks at 579.08 and 588.68 eV) species are present in the sample [34].

The XPS spectra of spent 2.5VZr (after O_2-ODH) and 2.5CrZr (after CO_2-ODH) catalysts are shown in Fig. 2S of supplementary information file. The spectra show that in the spent 2.5VZr catalyst two types of species are present, V^{+5} and V^{+3}. The full-width at half maximum (FWHM) of the V^{+5} were similar in the fresh and spent 2.5VZr catalyst. In contrast, the spent 2.5CrZr catalyst shows the presence of Cr^{+3} only. However, the FWHM of the Cr^{+3} species in the fresh and spent catalyst were different, which may be because we have used a single Cr^{+3} peak for our analysis. More recent studies have taken into consideration a main peak and multiple splitting peaks for analysis of the Cr^{+3} peak [23]. Thus, the oxidation state changes for the two catalysts in the two

Table 1
Characterization information of ZrO_2 supported vanadia and chromia catalysts: surface area, T_{max} and H/V ratio.

Catalyst	Surface area (m^2/g)	T_{max} (°C)	H/V ratio	Catalyst	Surface area (m^2/g)	T_{max} (°C)	H/Cr ratio
ZrO_2	48	-	-				
1VZr	46	438	2.15	1CrZr	45	295	2.44
2VZr	45	421	2.16	2CrZr	44	298	2.12
2.5VZr	44	430	2.18	2.5CrZr	43	294	2.06
3VZr	43	441	2.12	3CrZr	42	297	1.88

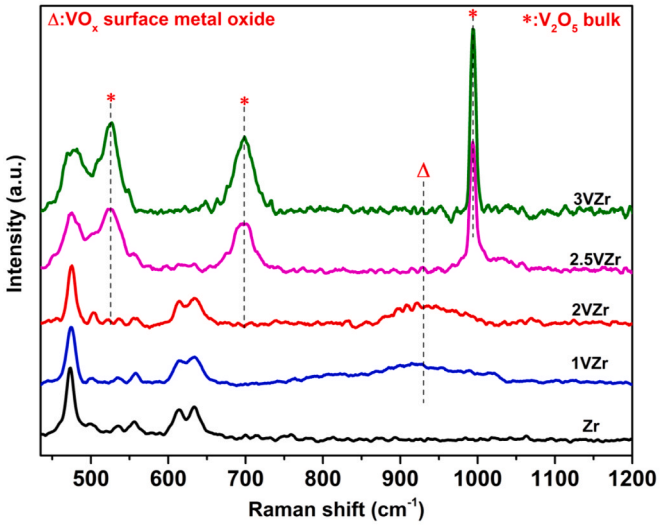

Fig. 1. Raman spectra of xVZr catalyst showing the presence of molecularly dispersed vanadia species and the transition from less than monolayer to more than monolayer coverages.

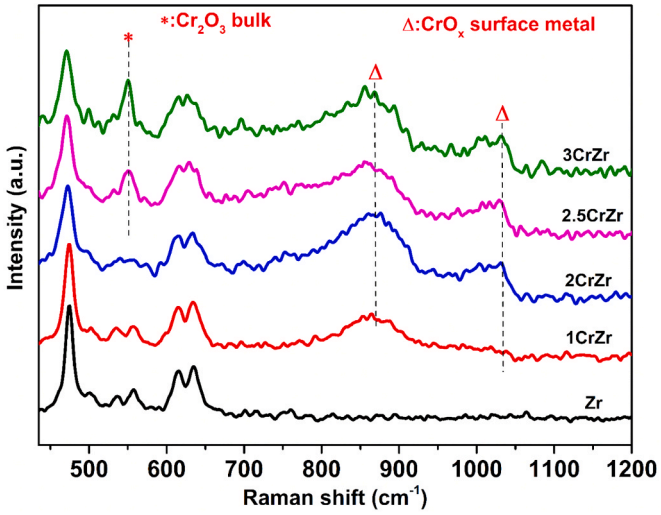

Fig. 2. Raman spectra of xCrZr catalyst showing the presence of molecularly dispersed chromia species and the transition from less than monolayer to more than monolayer coverages.

ODH reactions appear different.

3.4. H_2-TPR

All the prepared samples are characterized by H_2-TPR. The temperature at which TCD shows the highest signal is often referred to as T_{max}. All the catalysts used in the study showed a single T_{max}, which suggests that there is a single reduction step of the catalysts and the position of T_{max} depends on the support–surface metal oxide interaction [32,35]. The T_{max} of the xVZr and xCrZr samples are also tabulated in Table 1. The T_{max} of the xVZr samples are in the range of 421–441 °C, and of the xCrZr samples are in the range of 294–298 °C. The area under the curve is related to the H_2-TPR profile showing the H_2 uptake by the catalyst. With this data, the H/V ratios are calculated, and these values are between 2.18 and 2.12, as given in Table 1. Such H/V ratios suggest a reduction of V^{+5} to V^{+3} [17].

The xCrZr catalysts also show a single-step reduction and the T_{max} ranges from 294 to 298 °C. In contrast to the supported vanadia catalysts, for the xCrZr catalysts, the H/Cr ratio decreases from 2.44 to 1.88 as the metal loading increases. A H/Cr ratio of 3 would suggest a change in oxidation state from +6 to +3. Assuming the final oxidation state to be +3, which appears reasonable based on the XPS spectra discussed above, a value lower than 3 would imply that the initial oxidation state was not entirely +6. The 2.5CrZr catalyst indeed has Cr_2O_3 present, which has chromium in the +3 oxidation state. However, for sub-monolayer CrZr catalysts oxidation state lower than +6 is not evident. A previous study dealing with a series of ZrO_2 supported chromia catalysts revealed that the T_{max} ranges from 344 to 368 °C and the H/Cr ratio decreases with increasing loading [36]. The difference in the T_{max} temperature may be due to the difference in the source of ZrO_2 and/or the precursor and synthesis method used in the two studies. Furthermore, for Al_2O_3, TiO_2, SiO_2, and SiO_2-Al_2O_3 supported chromia catalysts, the T_{max} ranged from 388 to 373 °C, 351–342 °C, 445–435 °C and 380–365 °C, and the H/Cr ratio also decreased with an increase in chromia loading [32].

3.5. Reaction data for ODH of propane

3.5.1. Effect of metal oxide

Initially, sub-monolayer vanadia and chromia catalysts of equal loading were tested for O_2 ODH and CO_2 ODH at 550 °C and stoichiometric ratios of C_3H_8/oxidant. The partial pressure of C_3H_8 was kept constant at 0.075 atm for comparison.

3.5.1.1. O_2 ODH. The reaction results of O_2-ODH using 2VZr and 2CrZr for 2 h time-on-stream (TOS) are shown in Fig. 3. Tabulated values of the conversions and yields are given in Table 2S of the supplementary information file. Fig. 3 shows that the conversion of C_3H_8 and yield of C_3H_6 gradually declines with TOS for both catalysts; however, the decline in these two reactivity parameters is small. Further, 2VZr is more active than 2CrZr for O_2-ODH. The difference between the C_3H_8 conversion and C_3H_6 yield is the yield of CO+CO_2. The selectivity of C_3H_6 is nearly 28% for 2VZr and 30% for 2CrZr. Thus, the xVZr set of catalysts is used for additional studies on O_2-ODH.

3.5.1.2. CO_2 ODH. The CO_2 ODH reaction results with TOS for 2VZr and 2CrZr are shown in Fig. 4 and Fig. 3S of supplementary information file. Tabulated values of the conversions and yields are given in Table 3S of the supplementary information file. Similar to the O_2-ODH reaction, here also the conversions and yields decrease gradually with TOS and the decrease is small. However, for CO_2-ODH the 2CrZr catalyst converts more C_3H_8 and produces more C_3H_6 than 2VZr. The C_3H_6 selectivity was found to be 70% for 2VZr and 87% for 2CrZr.

In addition to the C_3H_8 conversion and C_3H_6 yield, the CO_2

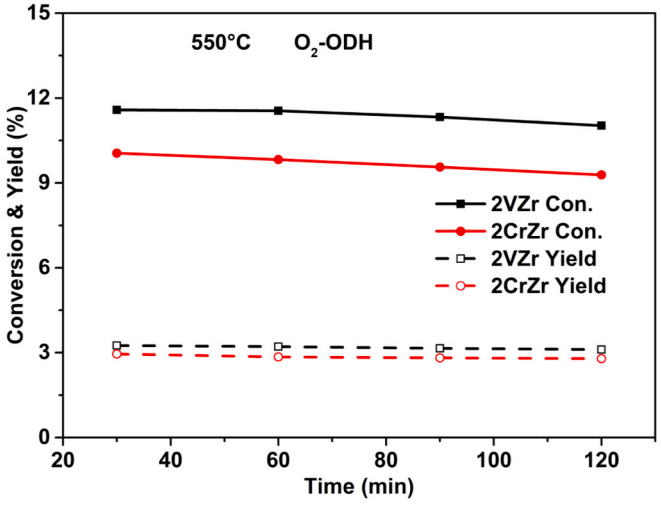

Fig. 3. C_3H_8 conversion and C_3H_6 yield for O_2-ODH of propane over 2VZr and 2CrZr as a function of TOS. Reaction conditions: Temperature 550 °C, Total pressure = 1 atm, $W/F_{C3H8,0}$ = 16.59 g.h/mol, $P_{C3H8,0}$ = 0.075 atm, $P_{O2,0}$ = 0.0375, balance N_2.

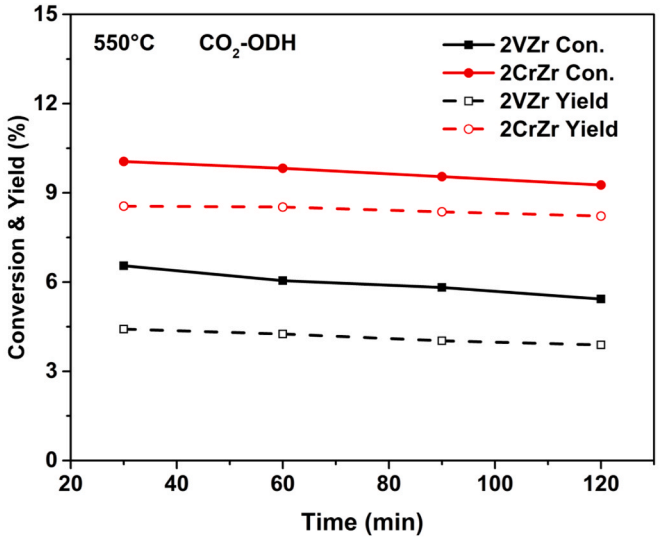

Fig. 4. C_3H_8 conversion and C_3H_6 yield for CO_2-ODH of propane over 2VZr and 2CrZr as a function of TOS. Reaction conditions: Temperature 550 °C, Total pressure = 1 atm, $W/F_{C3H8,0}$ = 16.59 g.h/mol, $P_{C3H8,0}$ = 0.075 atm, $P_{CO2,0}$ = $P_{C3H8,0}$, balance N_2.

conversion and CO yield are shown in Fig. 3S of supplementary information file. The CO_2 conversion also decreases with TOS and the decrease appears more rapid than the decrease in C_3H_8 conversion. In contrast, the CO yield appears to be more stable with TOS for both catalysts. Furthermore, the CO_2 conversion and CO yields are higher for 2CrZr compared to 2VZr. Based on the above observations we use the xCrZr set of catalysts for addition studies on CO_2-ODH.

3.5.2. *Effect of metal loading*

Metal oxide loading affects the catalytic activity of O_2-ODH and CO_2-ODH reactions [34]. To examine such effects the O_2-ODH and CO_2-ODH reactions were carried out over xVZr and xCrZr catalysts, respectively.

3.5.2.1. O_2-ODH over xVZr. The effect of vanadia loading for O_2-ODH reaction is shown in Fig. 5. Tabulated values of the conversions and yields are given in Table 2S of the supplementary information file. The

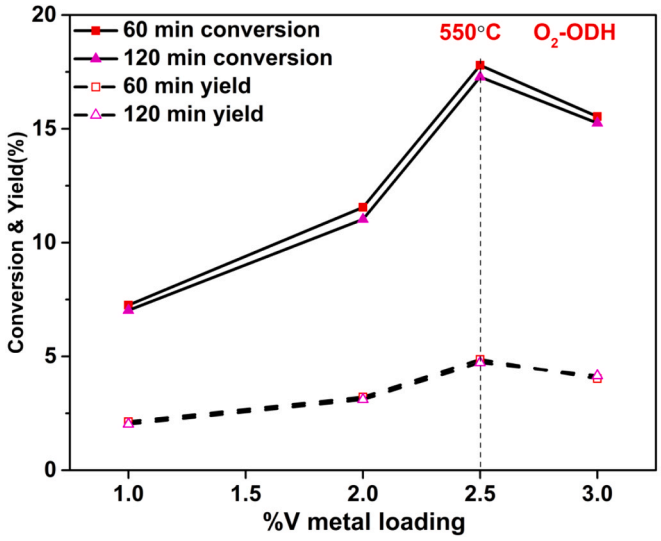

Fig. 5. C_3H_8 conversion and C_3H_6 yield for O_2-ODH of propane over xVZr catalysts. Reaction conditions: Temperature 550 °C, Total pressure = 1 atm, $W/F_{C3H8,0}$ = 16.59 g.h/mol, $P_{C3H8,0}$ = 0.075 atm, $P_{O2,0}$ = 0.0375, balance N_2.

conversion of C_3H_8 increases with loading from 7.3% and reaches a maximum of 17.8% for the 2.5VZr catalysts. The same trend is also observed for the yield of C_3H_6 and a maximum C_3H_6 yield of about 4.8% is observed for the 2.5VZr sample. The increase in C_3H_8 conversion and C_3H_6 yield up to 2.5% loading is consistent with an increase in the availability of molecularly dispersed species as observed by Raman spectroscopy. Above 2.5% monolayer loadings were exceeded since crystalline V_2O_5 was detected, and the conversion and yield decreased. It is clear that under the present operating conditions, the molecularly dispersed species are more active than crystalline V_2O_5.

3.5.2.2. CO_2-ODH over xCrZr. Similar to O_2-ODH, the C_3H_8 conversions, and C_3H_6 yields increase with chromium loading for the CO_2-ODH reaction and reach a maximum of 2.5%CrZr, as shown in Fig. 6. Tabulated values of the conversions and yields are given in Table 3S of the supplementary information file. For loadings above 2.5%, the C_3H_8 conversion and C_3H_6 yield decreases. The decrease in conversion and yield above 2.5% loading occurs since monolayer coverage is exceeded,

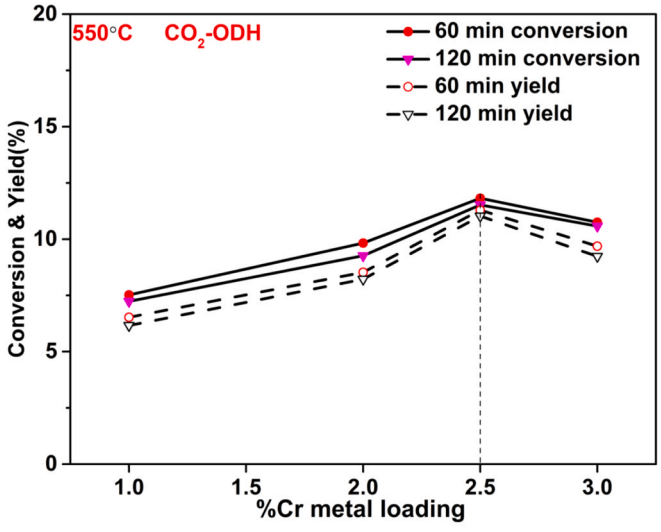

Fig. 6. C_3H_8 conversion and C_3H_6 yield for CO_2-ODH of propane over xCrZr catalysts. Reaction conditions: Temperature 550 °C, Total pressure = 1 atm, $W/F_{C3H8,0}$ = 16.59 g.h/mol, $P_{C3H8,0}$ = 0.075 atm, $P_{CO2,0}$ = $P_{C3H8,0}$, balance N_2.

as seen by Raman spectroscopy.

The CO_2 conversions and CO yields for the CO_2-ODH reaction using xCrZr catalysts are shown in Fig. 4S of supplementary information file. Similar to Fig. 6, the CO_2 conversions and CO yields increase up to 2.5% and then decrease. Furthermore, the conversions of C_3H_8 and CO_2 are similar, which is consistent with the stoichiometry of the CO_2-ODH reaction given by reaction (2). Thus, for both the xVZr and xCrZr sets of catalysts, it is evident that crystalline V_2O_5 and Cr_2O_3 are not as active as the corresponding molecularly dispersed species, and optimum conversions and yields are achieved for near monolayer loadings of vanadia and chromia.

From the data given in Figs. 5 and 6 the $TOF_{C_3H_8}$ and $TOF_{C_3H_6}$ were calculated based on the H_2-uptake data from H_2 TPR and tabulated in Table 2. The corresponding table for $TOF_{C_3H_8}$ and $TOF_{C_3H_6}$ based on the total moles of metal is given in Table 1S in the supplementary section. Similar trends in $TOF_{C_3H_8}$ and $TOF_{C_3H_6}$ are observed in Table 2 and Table 1S. Analyzing the data in Table 2 reveals that with change in the loading, no significant effect in the $TOF_{C_3H_8}$ and $TOF_{C_3H_6}$ is observed. It is evident that per active site the $TOF_{C_3H_8}$ is slightly higher for O_2-ODH over VZr compared to CO_2-ODH over CrZr. However, the $TOF_{C_3H_6}$ for CO_2-ODH over CrZr is significantly higher than for O_2-ODH over VZr. Thus, under these operating conditions, CO_2-ODH over CrZr is more suitable to produce propene.

3.5.3. *Effect of contact time*

The effect of contact time on the conversion, yield and selectivity for the best performing catalysts from section 3.4.1 is then examined.

3.5.3.1. O_2 ODH. The effect of increasing the contact time for the O_2-ODH reaction taking place at 550 °C using the 2.5VZrO_2 catalyst is shown in Fig. 7. As expected, the conversion of C_3H_8 increases rapidly. However, the C_3H_6 yield appears to increase gradually, and the main product formed is the undesirable carbon oxides. The C_3H_6 selectivity of about 30% is similar for all conversion values of C_3H_8, with slightly better selectivity at lower conversion values. Previous studies of supported vanadia catalysts do show higher C_3H_6 selectivity values [11]. However, these studies were carried out at lower temperatures, where the formation of the carbon oxide is less facilitated. We have also tested 2.5VZr for O_2-ODH at 400 °C using an inlet ratio of C_3H_8/O_2 =3 and the selectivity towards C_3H_6 was about 35%. At these temperatures of about 400 °C the Mars-van Krevelen mechanism occurs [11,37]. However, at higher temperatures, the presence of V^{+3}, as seen by from the XPS spectra, may also give rise to the DH of propane. Thus, carrying out the O_2-ODH at higher temperatures is not desirable over VZr catalysts since the selectivity towards C_3H_6 are severely compromised.

3.5.3.2. CO_2 ODH. The effect of contact time on the conversions and yields of CO_2-ODH using 2.5CrZr is shown in Fig. 8 and Fig. 5S of supplementary information file. In contrast to the O_2-ODH results, for CO_2-ODH the conversion increases steadily and appears to approach about 16% C_3H_8 conversion at high contact times. The C_3H_6 yield also increases and is always less than the C_3H_8 conversion values. At high contact times, a C_3H_6 yield of 13.7% and selectivity of 86.6% is achieved. The difference between C_3H_8 conversion and C_3H_6 yield appears to be related to amount of carbon being deposited, which increases with an increase in contact time.

With an increase in contact time, the CO_2 conversion and CO yield also monotonically increase and approach values of 16.1% and 17.3%, as seen in Fig. 5S of supplementary information file. Interestingly, the CO yield is greater than CO_2 conversions at high contact times. The excess of CO formed may be due to the reaction of CO_2 with surface carbon, $CO_2(g) + C(s) \rightarrow 2CO$. The surface carbon being formed from C_3H_8 and is not accounted for in the formula for CO yield given in Eq. (6)

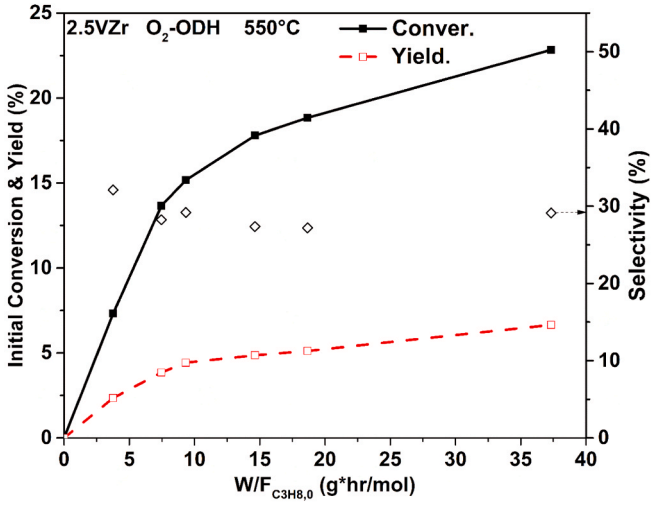

Fig. 7. C_3H_8 conversion, C_3H_6 yield and C_3H_6 selectivity for O_2-ODH of propane over 2.5VZr catalysts as a function of contact time ($W/F_{C3H8,0}$). Reaction conditions: Temperature 550 °C, Total pressure = 1 atm, $P_{C3H8,0}$ = 0.075 atm, $P_{O2,0}$ = 0.5 $P_{C3H8,0}$, balance N_2.

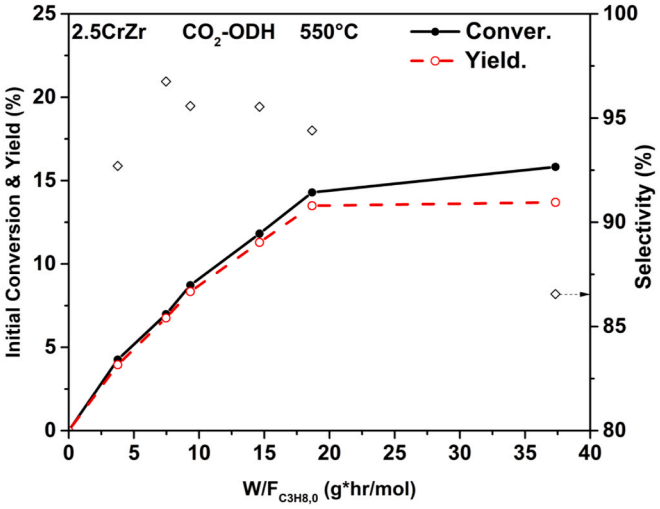

Fig. 8. C_3H_8 conversion, C_3H_6 yield, and C_3H_6 selectivity for CO_2-ODH of propane over 2.5CrZr catalysts as a function of contact time ($W/F_{C3H8,0}$). Reaction conditions: Temperature 550 °C, Total pressure = 1 atm, $P_{C3H8,0}$ = 0.075 atm, $P_{CO2,0}$ = $P_{C3H8,0}$, balance N_2.

Table 2
Turn-over frequency (TOF) values based on H_2-uptake & initial (0.5 h) conversion and yield of C_3H_8 and C_3H_6.

O_2 − ODH			*CO_2 − ODH*		
Catalyst	$TOF_{C3H8} * 10^{-3}$	$TOF_{C3H6} * 10^{-3}$	**Catalyst**	$TOF_{C3H8} * 10^{-3}$	$TOF_{C3H6} * 10^{-3}$
1VZr	**5.9**	**1.8**	**1CrZr**	**5.6**	**4.8**
2VZr	**4.6**	**1.3**	**2CrZr**	**4.1**	**3.6**
2.5VZr	**5.7**	**1.6**	**2.5CrZr**	**4.1**	**3.9**
3VZr	**4.2**	**1.2**	**3CrZr**	**3.4**	**3.1**

above. Furthermore, the similar conversion values of C_3H_8 and CO_2, which was also seen above, suggests that the predominant occurrence of the CO_2-ODH reaction rather than the dry reforming of C_3H_8, which has a stoichiometry of $C_3H_8 + 3CO_2 \rightarrow 6CO + 4H_2$. The dry reforming of C_3H_8 is one of the possible reactions that might occur when CO_2 and C_3H_8 are used as reactants, as suggested previously [7].

4. Conclusions

In the present study, we were able to successfully compare ZrO_2 supported vanadia and chromia catalysts for the O_2 and CO_2 assisted ODH of propane reaction. Monolayer loadings on this ZrO_2 support were determined to be between 2 and 2.5 wt%, which corresponds to coverages of 5.1–6.7 V-atoms/nm^2 and 5.2–6.6 Cr-atoms/nm^2. Using sub-monolayer catalysts, it was established that the molecularly dispersed vanadia species was more active during O_2-ODH and chromia species was more active for CO_2-ODH. However, the propene selectivity during O_2-ODH was low (~30%); whereas, the propene selectivity during CO_2-ODH was higher (~87%). The effect of vanadia loading for O_2-ODH and chromia loading for CO_2-ODH revealed that near monolayer coverages provided the highest propane conversion and propene yield, and that the molecularly dispersed species were more active than the crystalline counterparts. Furthermore, the CO_2 conversion and CO yield during CO_2-ODH was also the highest for the near monolayer chromia catalyst. The conversions of C_3H_6 and CO_2 were similar during CO_2-ODH suggesting the negligible occurrence of the CO_2 reforming of propane reaction. Furthermore, it appears that CO_2 is also involved with converting surface carbon to CO. With increase in contact time the O_2-ODH and CO_2-ODH reactions revealed an increase in propane conversion. However, during O_2-ODH the propene selectivity was relatively constant and continued to be low; whereas during CO_2-ODH, the propene selectivity gradually decreased from 86% to 94% due to carbon formation.

CRediT authorship contribution statement

Rajvikram Singh: Writing – original draft, Visualization, Validation, Software, Methodology, Investigation, Formal analysis, Data curation, Conceptualization. **Raghvendra Singh:** Writing – review & editing, Supervision, Resources, Project administration, Funding acquisition. **Sudhir Charan Nayak:** Resources. **Goutam Deo:** Writing – review & editing, Supervision, Resources, Project administration, Funding acquisition, Conceptualization.

Declaration of Competing Interest

The authors declare that they have no known competing financial interests or personal relationships that could have appeared to influence the work reported in this paper.

Data Availability

Data will be made available on request.

Acknowledgement

The authors acknowledge this special issue is dedicated to honor the 10th International Symposium on Group V (IV-VI) Elements, a gathering of international researchers, industry, young researchers and students to help shape the vision of the future for these elements. Further, Rajvikram Singh gratefully acknowledges the financial support from the IIT Kanpur and Ministry of Education (MoE).

Appendix A. Supporting information

Supplementary data associated with this article can be found in the online version at doi:10.1016/j.cattod.2024.114617.

References

[1] S. Chen, X. Chang, G. Sun, T. Zhang, Y. Xu, Y. Wang, C. Pei, J. Gong, Propane dehydrogenation: catalyst development, new chemistry, and emerging technologies, Chem. Soc. Rev. 50 (2021) 3315–3354, https://doi.org/10.1039/d0cs00814a.
[2] KM : PROPYLENE MARKET, 2015.
[3] U. Department of Energy, Chapter 6: Innovating Clean Energy Technologies in Advanced Manufacturing, 2015.
[4] I. Amghizar, L.A. Vandewalle, K.M. Van Geem, G.B. Marin, New trends in olefin production, Engineering 3 (2017) 171–178, https://doi.org/10.1016/J.ENG.2017.02.006.
[5] F. Cavani, N. Ballarini, A. Cericola, Oxidative dehydrogenation of ethane and propane: How far from commercial implementation? Catal. Today 127 (2007) 113–131, https://doi.org/10.1016/j.cattod.2007.05.009.
[6] X. Jiang, L. Sharma, V. Fung, S.J. Park, C.W. Jones, B.G. Sumpter, J. Baltrusaitis, Z. Wu, Oxidative dehydrogenation of propane to propylene with soft oxidants via heterogeneous catalysis, ACS Catal. 11 (2021) 2182–2234, https://doi.org/10.1021/acscatal.0c03999.
[7] Y. Gambo, S. Adamu, G. Tanimu, I.M. Abdullahi, R.A. Lucky, M.S. Ba-Shammakh, MohammadM. Hossain, CO2-mediated oxidative dehydrogenation of light alkanes to olefins: advances and perspectives in catalyst design and process improvement, Appl. Catal. A Gen. 623 (2021) 118273, https://doi.org/10.1016/j.apcata.2021.118273.
[8] M.A. Atanga, F. Rezaei, A. Jawad, M. Fitch, A.A. Rownaghi, Oxidative dehydrogenation of propane to propylene with carbon dioxide, Appl. Catal. B 220 (2018) 429–445, https://doi.org/10.1016/j.apcatb.2017.08.052.
[9] D. Chen, A. Holmen, Z. Sui, X. Zhou, Carbon mediated catalysis: a review on oxidative dehydrogenation, Chin. J. Catal. 35 (2014) 824–841, https://doi.org/10.1016/S1872-2067(14)60120-0.
[10] J.H. Carter, T. Bere, J.R. Pitchers, D.G. Hewes, B.D. Vandegehuchte, C.J. Kiely, S. H. Taylor, G.J. Hutchings, Direct and oxidative dehydrogenation of propane: from catalyst design to industrial application, Green Chem. 23 (2021) 9747–9799, https://doi.org/10.1039/D1GC03700E.
[11] C.A. Carrero, R. Schloegl, I.E. Wachs, R. Schomaecker, Critical literature review of the kinetics for the oxidative dehydrogenation of propane over well-defined supported vanadium oxide catalysts, ACS Catal. 4 (2014) 3357–3380, https://doi.org/10.1021/cs5003417.
[12] J.J.H.B. Sattler, J. Ruiz-Martinez, E. Santillan-Jimenez, B.M. Weckhuysen, Catalytic dehydrogenation of light alkanes on metals and metal oxides, Chem. Rev. 114 (2014) 10613–10653, https://doi.org/10.1021/cr5002436.
[13] I.E. Wachs, Raman and IR studies of surface metal oxide species on oxide supports: Supported metal oxide catalysts, Catal. Today 27 (1996) 43–455, https://doi.org/10.1016/0920-5861(95)00203-0.
[14] J. Strunk, M.A. Bañares, I.E. Wachs, Vibrational spectroscopy of oxide overlayers, Top. Catal. 60 (2017) 1577–1617, https://doi.org/10.1007/s11244-017-0841-x.
[15] I.E. Wachs, Catalysis science of supported vanadium oxide catalysts, Dalton Trans. 42 (2013) 11762–11769, https://doi.org/10.1039/c3dt50692d.
[16] M.A. Bañares, I.E. Wachs, Molecular structures of supported metal oxide catalysts under different environments, J. Raman Spectrosc. 33 (2002) 359–380, https://doi.org/10.1002/jrs.866.
[17] I.E. Wachs, Y. Chen, J.-M. Jehng, L.E. Briand, T. Tanaka, Molecular structure and reactivity of the Group V metal oxides, Catal. Today 78 (2003) 13–24, https://doi.org/10.1016/S0920-5861(02)00337-1.
[18] X. Ge, H. Zou, J. Wang, J. Shen, Modification of Cr/SiO2 for the dehydrogenation of propane to propylene in carbon dioxide, React. Kinet. Catal. Lett. 85 (2005) 253–260.
[19] B. Mitra, I.E. Wachs, G. Deo, Promotion of the propane ODH reaction over supported V2O5/Al2O3 catalyst with secondary surface metal oxide additives, J. Catal. 240 (2006) 151–159, https://doi.org/10.1016/j.jcat.2006.03.015.
[20] A.S. Sandupatla, K. Ray, P. Thaosen, C. Sivananda, G. Deo, Oxidative dehydrogenation of propane over alumina supported vanadia catalyst – Effect of carbon dioxide and secondary surface metal oxide additive, Catal. Today 354 (2020) 176–182, https://doi.org/10.1016/j.cattod.2019.06.047.
[21] S.S. Chan, I.E. Wachs, L.L. Murrell, L. Wang, W.K. Hall, Situ Laser Raman Spectrosc. Support. Met. Oxides (1984). ⟨https://pubs.acs.org/sharingguidelines⟩.
[22] A.E. Lewandowska, M.A. Bañares, In situ TPR/TPO-Raman studies of dispersed and nano-scaled mixed V-Nb oxides on alumina, Catal. Today 118 (2006) 323–331, https://doi.org/10.1016/j.cattod.2006.07.014.
[23] G. do, N. Franceschini, P. Concepción, M. Schwaab, M. do Carmo Rangel, J. Martínez-Triguero, J.M. López Nieto, Spectroscopic insights into the role of CO2 on the nature of Cr species in a CrOX/Al2O3 catalysts during ethane dehydrogenation with CO2, Appl. Catal. A Gen. 661 (2023), https://doi.org/10.1016/j.apcata.2023.119260.
[24] T.V. Malleswara Rao, G. Deo, J.M. Jehng, I.E. Wachs, In situ UV-Vis-NIR diffuse reflectance and raman spectroscopy and catalytic activity studies of propane oxidative dehydrogenation over supported CrO 3/ZrO 2 catalysts, Langmuir 20 (2004) 7159–7165, https://doi.org/10.1021/la049590v.
[25] C.L. Pieck, M.A. Bañares, J.L.G. Fierro, Propane oxidative dehydrogenation on VOx/ZrO2 catalysts, J. Catal. 224 (2004) 1–7, https://doi.org/10.1016/j.jcat.2004.02.024.
[26] J. Liu, Z. Zhao, C. Xu, A. Duan, G. Jiang, J. Gao, W. Lin, I.E. Wachs, In-situ UV-Raman study on soot combustion over TiO2 or ZrO 2-supported vanadium oxide catalysts, Sci. China B Chem. 51 (2008) 551–561, https://doi.org/10.1007/s11426-008-0027-2.

[27] C.L. Pieck, M.A. Bañares, M.A. Vicente, J.L.G. Fierro, Chemical structures of ZrO2-supported V - Sb oxides, Chem. Mater. 13 (2001) 1174–1180, https://doi.org/10.1021/cm000333v.
[28] F. Roozeboom, M.C. Mltlelmeljer-Hazeleger, J.A. Moulijn, J. Moderna, V.H.J. De Beer, P.J. Sellings, A Raman Spectroscopic and Temperature-Programmed Reduction Study of Monolayer and Crystal-Type Vanadia on Various Supports 12, 1980. ⟨https://pubs.acs.org/sharingguidelines⟩.
[29] N. Das, H. Eckert, H. Hu, I.E. Wachs, J.F. Walzer, F.J. Feher, Bonding States of Surface Vanadium(V) Oxide Phases on Silica: Structural Characterization by 5IV NMR and Raman Spectroscopy, 1993. ⟨https://pubs.acs.org/sharingguidelines⟩.
[30] A. Khodakov, B. Olthof, A.T. Bell, E. Iglesia, Structure and Catalytic Properties of Supported Vanadium Oxides: Support Effects on Oxidative Dehydrogenation Reactions The effects of support (Al, 1999. ⟨http://www.idealibrary.comon⟩.
[31] F.D. Hardcastle, I.E. Wachs, Raman spectroscopy of chromium oxide supported on Al2O3, TiO2 and SiO2: a comparative study, J. Mol. Catal. 46 (1998) 173–186, https://doi.org/10.1016/0304-5102(88)85092-2.
[32] M. Cherian, M.S. Rao, A.M. Hirt, I.E. Wachs, G. Deo, Oxidative dehydrogenation of propane over supported chromia catalysts: Influence of oxide supports and chromia loading, J. Catal. 211 (2002) 482–495, https://doi.org/10.1006/jcat.2002.3759.
[33] J.F.S. de Oliveira, D.P. Volanti, J.M.C. Bueno, A.P. Ferreira, Effect of CO2 in the oxidative dehydrogenation reaction of propane over Cr/ZrO2 catalysts, Appl. Catal. A Gen. 558 (2018) 55–66, https://doi.org/10.1016/j.apcata.2018.03.020.
[34] Z. Xie, Y. Ren, J. Li, Z. Zhao, X. Fan, B. Liu, W. Song, L. Kong, X. Xiao, J. Liu, G. Jiang, Facile in situ synthesis of highly dispersed chromium oxide incorporated into mesoporous ZrO2 for the dehydrogenation of propane with CO2, J. Catal. 372 (2019) 206–216, https://doi.org/10.1016/j.jcat.2019.02.026.
[35] G. Deo, I.E. Wachs, Reactivity of supported vanadium oxide catalysts the partial oxidation of methanol, J. Catal. 146 (1994) 323–334, https://doi.org/10.1006/jcat.1994.1071.
[36] D.L. Hoang, H. Lieske, Temperature-programmed reduction study of chromium oxide supported on zirconia and lanthana-zirconia, Thermochim. Acta 345 (2000) 93–99, https://doi.org/10.1016/S0040-6031(99)00385-8.
[37] J.J. Ternero-Hidalgo, M. Daturi, G. Clet, P. Bazin, M.A. Bañares, R. Portela, M. O. Guerrero-Pérez, J. Rodríguez-Mirasol, T. Cordero, A simultaneous operando FTIR & Raman study of propane ODH mechanism over V-Zr-O catalysts, Catal. Today 387 (2022) 197–206, https://doi.org/10.1016/j.cattod.2021.06.012.